Assessment of coupling conditions in water way intersections

Michael Herty[1,*] and Mohammed Seaïd[2,†]

[1] *RWTH Aachen University, Templergraben 55, D-52056 Aachen, Germany*
[2] *School of Engineering and Computing Sciences, University of Durham, South Road, Durham DH1 3LE, UK*

SUMMARY

We present a numerical assessment of coupling conditions in T-junction for water flow in open canals. The mathematical model is based on the well-established shallow water equations for open channel flows. In the present work, the emphasis is given to the description of coupling conditions at canal-to-canal intersections. The accurate prediction of these coupling conditions is essential in order to achieve good performance and reliable numerical simulations of water canals in networks. There is exists several theoretical results for coupling conditions in a reduced geometry. The purpose of our work is to numerically verify these conditions for different water flow regimes. More precisely, we consider a local zooming of the T-junction resulting in a two-dimensional flow problem at the canals intersection. A high-order non-oscillatory method is used for solving the governing two-dimensional equations and the water flow solutions are space-averaged over the junction areas. The obtained numerical results are thereafter, used for verification and comparison with the theoretical results. Verifications are conducted for two types of junctions namely the 1-to-2 and 2-to-1 situations.

KEY WORDS: Water canals; shallow water equations; T-junction; coupling conditions; networks

1. Introduction

During the last decade, there has been intense research in the field of transportation networks in the mathematical as well as in the engineering community. Here, we are particularly interested in networks of open canals and coupling conditions at water way intersections. Besides work on the dynamics governing the water flow inside a canal, most of the recent works is focused on the correct modeling and simulation of canal-to-canal junctions based on the well-established shallow water equations in one space dimension, see for example [8, 9, 11, 12, 13, 14, 15, 16, 24, 25, 26]. Some of the cited references also include control aspects for nodal optimization at the canal-to-canal intersections. In all these works the canal junction is assumed to be a single point (zero length). To obtain a well-posed problem, coupling

*Correspondence to: herty@mathc.rwth-aachen.de
†E-mail: m.seaid@durham.ac.uk

conditions (with and without control action) at the fitting have to be derived. These conditions are then used as boundary conditions to the one-dimensional shallow water equations. A similar study has been carried out in the literature for the case of gas flow in pipeline networks governed by the so-called p-system. Indeed, for $\gamma = 2$ one obtains from a mathematical point of view the same system as the shallow water equations. Therefore, the discussion can be equivalently applied to gas and water flows in networks. Currently, different conditions have been proposed and discussed in the case of gas networks [4, 5, 7, 8]. For water networks extensive studies have been done in [6, 13, 17, 18] among others.

In this work we contribute to this discussion by a numerical study of an extended two-dimensional model. We investigate the detailed water flow dynamics at the tee fitting of different canal-to-canal intersections. We assume that the dynamics inside each canal are given by the shallow water equations and resolve the detailed dynamics inside different types of canal intersections with a robust numerical scheme as discussed below. The resolution is achieved by introducing a local zooming of the situation under study. This yields a two-dimensional domain representing the tee fitting with corresponding initial flow conditions in each canal. Therein, we simulate the water dynamics for a steady-state equilibrium and finally average the obtained flow solutions to obtain reference values at the T-junction. The obtained values are then compared to boundary values commonly used for the one-dimensional shallow water equations. We compare the simulation results with the analytical solutions which can be computed for constant states in the literature [14, 9]. Note that in our simulations no gate control is present and we only focus on intersections with three canals. Therefore the geometry is different to [6, 13].

In contrast to the comparison study performed for gas pipeline networks in [20], we consider in the current study the situation of small perturbations of a given initial data. Here, given an initial distribution of the water flow conditions at each canal, we introduce a perturbation of the water height and the discharge in one canal for the 1-to-2 situation and in two canals for the 2-to-1 canal situation. The study of local perturbations is a realistic scenario for large water canal networks which in general are subject to these perturbations due to rainfall, opening valves or flooding. We also modify the numerical procedures in order to treat the shallow water equations compared with the isothermal Euler equations in [20]. The discussion of the predictions of the theoretical results is modified in order to treat special coupling conditions appearing in water canals, namely equal water head or equal water pressure. An important issue is the selection of the numerical scheme, which accurately resolves the two-dimensional equations in the considered tee fittings. It is well known that the solutions of these equations present steep fronts, shocks and contact discontinuities, which need to be resolved accurately in applications and often cause severe numerical difficulties. High-order accurate schemes have become important in scientific computations because they offer a mean to obtain accurate solutions with less work that may be required for methods of lower accuracy. The literature is abundant for development of high-order methods for solving hyperbolic systems of conservation laws, among others we cite the Weighted Essentially Non-Oscillatory (WENO) methods, compare [2, 22] among others. In the current work we have implemented a fifth-order WENO scheme in the relaxation framework. First-order and second-order relaxation schemes have been studied in [3]. A variety of third-order relaxation schemes have also been developed in [30, 29, 28] for solving hyperbolic systems. The main advantage in considering combined relaxation WENO approach lies essentially on the semi-linear structure of the relaxation

system, which can be solved numerically without using Riemann solvers or characteristic decomposition.

This paper is structured as follows. In section 2 we formulate the governing equations for the water flow in canals. Section 3 is devoted to the discussion of coupling condition at T-junction in canal networks. Numerical methods and assessment procedure are briefly described in section 4. In section 5 we present numerical results for two types of junctions. Section 6 contains concluding remarks and remarks about future work.

2. Governing Equations for Water Flow in Canal Networks

The transient flow of water in canals can be adequately described by the one-dimensional approach. The basic equations modeling the water flow in canals are the well-established shallow water equations given by the continuity and momentum equations. For practical applications, the form of the governing equations varies with respect to the assumptions made. Simplified models are usually obtained by neglecting certain dynamical aspects of the physical process. In the current work, to keep the presentation simple, we assume that all canals have the same diameter D and constant cross-sectional area. Hence, the continuity equation for water flow in a canal k is given by

$$\partial_t h_k + \partial_x \left(h_k u_k \right) = 0, \tag{1}$$

where h_k and u_k are the water height and the water velocity in the canal k. The momentum equation for the water flow is

$$\partial_t \left(h_k u_k \right) + \partial_x \left(h_k u_k^2 + \frac{1}{2} g h_k^2 \right) = g h_k \left(S_0 - S_f \right), \tag{2}$$

where g is the gravitational acceleration, S_0 the bed slope and S_f the friction slope defined as

$$S_0 = -\partial_x B_k, \qquad S_f = n_k^2 \frac{u_k |u_k|}{R_k^{\frac{4}{3}}}, \tag{3}$$

with B_k represents the bottom topography of the canal k, n_k is the Manning roughness coefficient at the bed in the canal k and R_k is the hydraulics radius (ratio of cross-sectional area of the wetted perimeter in the the canal k). for the purpose of the present study, we assume a steady state friction on all canals and we assume horizontal canals with zero slope. Thus, the equations (1)-(2) can be reformulated in vector from as

$$\partial_t \mathbf{U}_k + \partial_x \mathbf{F} \left(\mathbf{U}_k \right) = \mathbf{0}, \tag{4}$$

where

$$\mathbf{U}_k = \begin{pmatrix} h_k \\ h_k u_k \end{pmatrix}, \qquad \mathbf{F}(\mathbf{U}_k) = \begin{pmatrix} h_k u_k \\ h_k u_k^2 + p_k \end{pmatrix},$$

with p_k is the water pressure defined by

$$p_k = \frac{1}{2} g h_k^2. \tag{5}$$

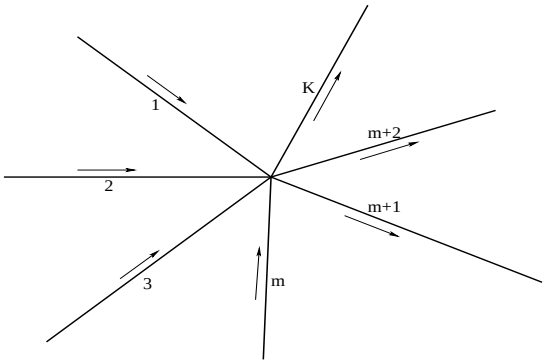

Figure 1. An illustration of canal-to-canal intersection in a network with $i = 1, \dots, m$ ingoing canals and $i = m + 1, \dots K$ outgoing canals.

The equations (1)-(2) describe transient water flow inside a canal k where $k = 1, \dots, K$, with K is the total number of canals in the network, compare Figure 1 for an illustration. We assume that each canal k is represented by an interval $[a_k, b_k]$ for $k = 1, \dots, K$. If a canal k is incoming or outgoing to the whole network we set $a_k = -\infty$ or $b_k = +\infty$, respectively. In addition, to simulate a canal network over a time interval $[0, T]$, the system (4) has to be complemented by initial data $\mathbf{U}_k = (h_k^0, u_k^0)^T$ and appropriate boundary conditions at $x = a_k$ or $x = b_k$. These conditions are subject to our discussion in the following section.

3. Coupling Conditions at the Canal-to-Canal Intersections

Recently, there has been a growth of interest in coupled systems of hyperbolic equations with applications to gas and water networks, see for example [4, 8, 13, 26, 14] for theoretical studies and [1, 20, 21] for numerical discussions. So far, the existing theoretical results treat the one-dimensional situation. In our context this amounts to assume that one each canal k the flow is governed by the shallow-water equations (4). Due to the finite speed of propagation the theoretical discussion can be restricted to the case of a single intersection (with some exceptions [16, 26]). Then, we may parameterize each canal k such that different canals are connected at $x = 0$. Typically, at $x = 0$ algebraic conditions are prescribed which couple the dynamics on different canals k and l. Examples of commonly used coupling conditions are:

Conservation of mass:

$$\sum_k h_k u_k = 0, \qquad \forall\, t > 0. \tag{6}$$

Equal water pressure:

$$\frac{1}{2} g h_k^2 = \frac{1}{2} g h_l^2, \qquad \forall\, t > 0. \tag{7}$$

Equal water head:

$$h_k + \frac{u_k^2}{2g} = h_l + \frac{u_l^2}{2g}, \qquad \forall\, t > 0. \tag{8}$$

Note that due to the parametrization all canals are pointing away from the intersection. Equivalently, we could parameterize the outgoing canals by $(0, \infty)$ and the incoming by $(-\infty, 0)$. Then, condition (6) is equivalent to

$$\sum_{k:\text{ incoming}} (hu)_k(0^-, t) = \sum_{l:\text{ outgoing}} (hu)_l(0^+, t), \qquad \forall\, t > 0.$$

The condition (7) prescribes an equal pressure at the intersection and is commonly used in gas networks as well as water engineering applications. The condition (8) yields an equal water head at the intersection. Further conditions, like conservation of momentum can be prescribed and have been discussed in the case of gas networks for example in [4, 7]. Note that the set of conditions (6) and (7) or (6) and (8) are imposed *a priori*. This is the case for the mathematical discussion as well as the case in all engineering applications [32].

Well-posedness of the different coupling conditions has been analyzed by various authors and we can only give an incomplete list of references [5, 9, 11, 14, 24] and offer only a partial discussion of some results. Nowadays, there exists results in two directions. Some works have been devoted to the case of smooth solutions, see for instance [14, 24, 12, 11, 13, 15, 16, 25, 26]. In this case the differentiation of the flux function is possible and after decomposition into characteristic variables the definition of incoming and outgoing boundary conditions for each canal is straightforward, compare for instance [14]. Additional questions of control and stabilization for the obtained systems in quasi-linear form has then been the major focus of recent works [24, 12, 13, 15, 16, 25, 26]. On the other hand, if one is interested in non-smooth solutions, a recent result on well-posedness for general strictly hyperbolic 2×2-systems has been established in [9, 10]. Results for particular coupling conditions can also be found for example in [5, 4, 7, 8]. In all these approaches the number of incoming and outgoing boundary conditions depends on the state of the system. The method to obtain a well-posed problem is then solved by introducing the so-called half-Riemann problems at the intersection. These problems differ from the classical Riemann problem in the following way: Assume a given constant initial data $U_k^{(0)}$ on each canal k and a set of coupling condition as for example (6) and (7) or (6) and (8). We then seek for intermediate values U^* fulfilling the coupling conditions. Furthermore, the values of U^* are chosen such that the Riemann problem formed by the equations (4) subject to the initial condition

$$U(x, 0) = \begin{cases} U^*, & \text{if} \quad x \leq 0, \\ \\ U_k^{(0)}, & \text{if} \quad x \geq 0, \end{cases} \tag{9}$$

admits a self-similar solution which consists of a superposition of waves traveling with *non-negative* speed. We therefore have $U(0^+, t) = U^*$ for $t > 0$ and hence the coupling conditions are satisfied. It has been proven that under suitable assumptions this procedure gives existence, uniqueness and Lipschitz dependence on the initial data for general 2×2-system of conservation laws and for rather general coupling conditions, we refer the reader to [9] for more details. The results of this discussion can be used in modified Riemann solvers for numerical purposes, see [5, 4, 1, 21] for a situation of two coupled gas pipes with different flux functions. This approach is similar to the solution of initial-boundary value problems for hyperbolic systems with the difference being that in the present case we additionally have to satisfy some algebraic conditions.

In the current work we are interested in a comparison with a simulation of a numerical two-dimensional situation. Since the simulations will include shock waves, we only compare the numerical results with the theoretical predictions obtained from studies of the Riemann problem at the junction. The aim of the presented simulations is to verify the imposed conditions (6) and (7) or (6) and (8), respectively. We simulate different inflow configurations for two types of tee intersections with three connected canals. In the second stage, we average the computed results to obtain equivalent one-dimensional fluxes, water heads and water pressures for each canal (referred to as simulation results in the sequel). These values will be compared with the states U^* obtained as in the discussion above (referred to as theoretical results in the sequel). Note that the theoretical results can be found by solving the following equations for a given state $U_k^{(0)}$ and given states U_k^p. We solve for $(h_k^*)_i$ the nonlinear system

$$\begin{aligned}\sum_k L_2^-\left(h_k^*;\left(h_k^p, L_1^+(h_k^p;U_k^{(0)})\right)\right) &= 0,\\ \frac{1}{2}g\,(h_k^*)^2 &= \frac{1}{2}g\,(h_l^*)^2, \qquad l\neq k,\end{aligned}$$

in the case of the coupling conditions (6) and (7), and

$$\begin{aligned}\sum_k L_2^-\left(h_k^*;\left(h_k^p, L_1^+(h_k^p;U_k^{(0)})\right)\right) &= 0,\\ h_k^* + \frac{\left(L_2^-\left(h_k^*;\left(h_k^p, L_1^+(h_k^p;U_k^{(0)})\right)\right)\right)^2}{2g(h_k^*)^2} &= h_l^* + \frac{\left(L_2^-\left(h_l^*;\left(h_l^p, L_1^+(h_l^p;U_0^j)\right)\right)\right)^2}{2g(h_l^*)^2},\end{aligned}$$

in the case of the coupling conditions (6) and (8), respectively. The states U_k^p are local perturbations of $U_k^{(0)}$ and their construction will be discussed below. The functions $L_{1,2}^{\pm}$ are the forward and reversed 1-Lax curve and 2-Lax curve for the shallow water equations defined by [8, 27]

$$L_1^+(h;(h_0,h_0u_0)) = \begin{cases} u_0h + 2h\left(\sqrt{gh_0}-\sqrt{gh}\right), & \text{if} \quad h\le h_0,\\ u_0h - h(h-h_0)\sqrt{\dfrac{g}{2}\left(\dfrac{1}{h}+\dfrac{1}{h_0}\right)}, & \text{if} \quad h>h_0,\end{cases}$$

and

$$L_2^-(h;(h_0,h_0u_0)) = \begin{cases} u_0h - 2h\left(\sqrt{gh_0}-\sqrt{gh}\right), & \text{if} \quad h\le h_0,\\ u_0h + h(h-h_0)\sqrt{\dfrac{g}{2}\left(\dfrac{1}{h}+\dfrac{1}{h_0}\right)}, & \text{if} \quad h>h_0.\end{cases}$$

The solution h_k^* together with $L_2^-\left(h_k^*;\left(h_k^p, L_1^+(h_k^p;U_0^k)\right)\right) = h_k^*u_k^*$ is the theoretical prediction for the one-dimensional situation. We present results for different perturbations starting from the steady-state $U_k^{(0)} = (1,0)^T$ at the junction. The perturbation U^p is chosen as follows:

We compute a state $U^p = (h^p,(hu)^p)^T$, such that the solution to a Riemann problem for the one-dimensional shallow water equations with left state U^p and right state $U = (1,0)^T$

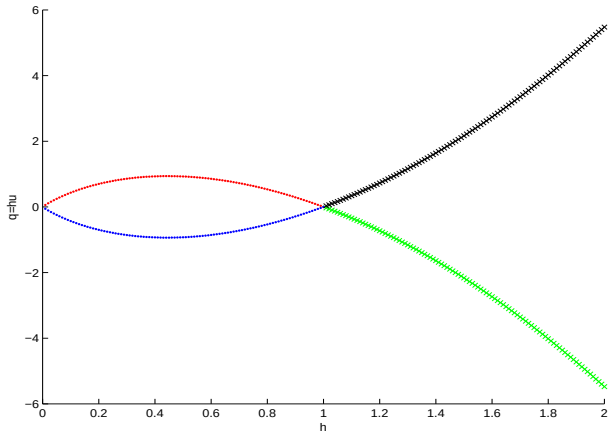

Figure 2. Characteristic curves through the state $U = (1, 0)^T$ for the shallow water equations (4). States on the black part of the curve can be connected to U by 2-shock waves of non-negative speed. States on the blue line up to $h = 0.5$ can be connected to U by 2-rarefaction waves of non-negative speed. The dotted part of the curves belong to states which are connected to U by rarefaction waves.

contains waves of non-negative speed only. These states are depicted in Figure 2 and belong to the reversed 2-Lax curve in the phase space (h, hu) which is given by

$$hu = \begin{cases} \sqrt{gh}(h-1)\sqrt{\dfrac{h+1}{2}}, & h > 1, \\ 2\sqrt{g}h\left(\sqrt{h}-1\right), & h < 1, \end{cases} \tag{10}$$

and the given (right) state $U = (1, 0)^T$. The solution to the Riemann problem formed by the equations (4) subject to the initial condition

$$\begin{pmatrix} h(x,0) \\ (hu)^0(x,0) \end{pmatrix} = \begin{cases} \begin{pmatrix} h^* \\ (hu)^* \end{pmatrix}, & \text{if} \quad x \le 0, \\ \begin{pmatrix} 1 \\ 0 \end{pmatrix}, & \text{if} \quad x \ge 0, \end{cases} \tag{11}$$

for any state $(h^p, (hu)^p)$ such that (10) is either a shock wave ($h^p > 1$) or a rarefaction wave ($h^p < 1$) with speed $\sqrt{\frac{1}{2}gh(h+1)} > 0$ or speed $u + \sqrt{gh} > 0$, respectively. Therefore, the prescribed perturbations will move towards the junction and modify the state there. The values after the perturbation interacted with the other states at the junction can be computed analytically in the one-dimensional situation. We report results for different coupling conditions below. For the numerical simulation of the two-dimensional model, we use the same perturbed state U^p and additionally prescribe the velocity in y-direction to be equal to zero.

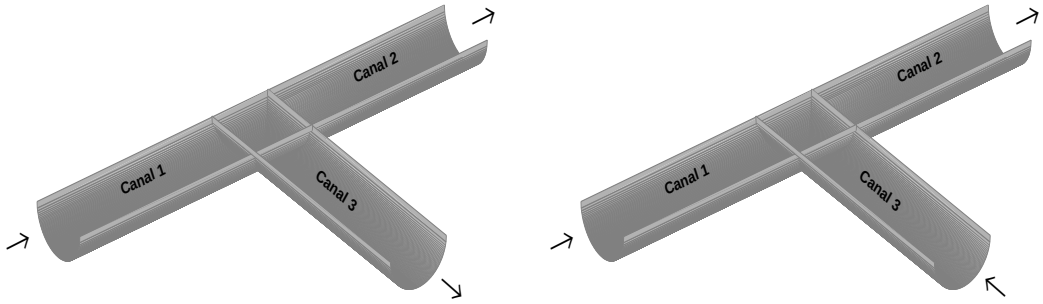

Figure 3. Schematic representation of two types of tee fittings and modeling in the network.

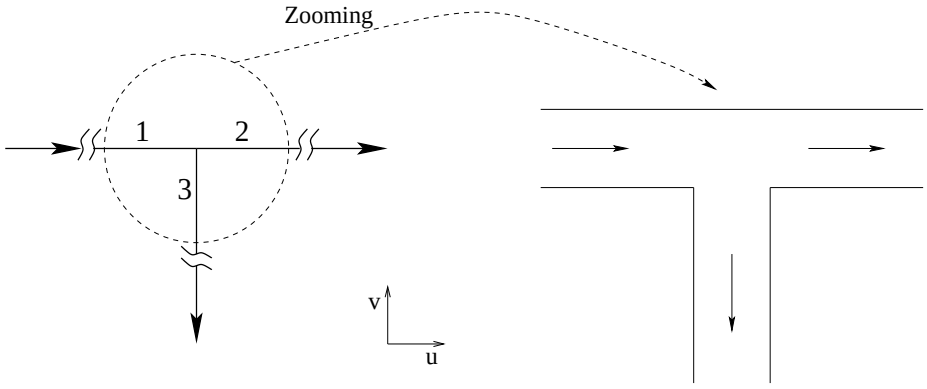

Figure 4. Zooming at a tee fittings and its corresponding two-dimensional domain.

4. Numerical Methods and Solution Procedure

To keep the presentation simple and to compare later with analytical results we restrict the discussion to tee fittings. We introduce a zooming of the local situation at the intersection and consider a local two-dimensional situation. The zooming width parameter to be introduced later is $\gamma > 0$. In the case of the tee fittings in Figure 3 we obtain the schematic picture shown in Figure 4, where the canal width is of order 2γ.

The governing equations in this T-shaped two dimensional domain are the two-dimensional frictionless shallow water equations on flat bottom

$$\begin{aligned} \partial_t h + \partial_x (hu) + \partial_y (hv) &= 0, \\ \partial_t (hu) + \partial_x \left(hu^2 + \frac{1}{2} g h^2 \right) + \partial_y (huv) &= 0, \\ \partial_t (hv) + \partial_x (huv) + \partial_y \left(hv^2 + \frac{1}{2} g h^2 \right) &= 0, \end{aligned} \tag{12}$$

where u and v are the velocity components in x- and y-direction, respectively. This two-dimensional view is now used to obtain boundary conditions for (4). As in the theory presented in [5] for the equations (4), we consider constant initial data ρ_k^0, u_k^0 for $k = 1, 2$ and 3. This data is used to define initial values for equation (12) as

$$\begin{pmatrix} h^0(x,y) \\ (hu)^0(x,y) \\ (hv)^0(x,y) \end{pmatrix} = \begin{cases} \begin{pmatrix} h_1^0 \\ (hu)_1^0 \\ 0 \end{pmatrix}, & \text{if} \quad (x,y) \in]-\infty, 0[\times]0, 2\gamma[, \\ \begin{pmatrix} h_3^0 \\ (hu)_3^0 \\ 0 \end{pmatrix}, & \text{if} \quad (x,y) \in]0, \infty[\times]0, 2\gamma[, \\ \begin{pmatrix} h_2^0 \\ 0 \\ (hu)_2^0 \end{pmatrix}, & \text{if} \quad (x,y) \in]-\gamma, \gamma[\times]-\infty, 0[. \end{cases} \tag{13}$$

Note, that 2γ is the width of the connected canals. We compute the steady-state solutions $h = h^\gamma(x,y)$, $(hu) = (hu)^\gamma(x,y)$, $(hv) = (hv)^\gamma(x,y)$ of (12)-(13) for fixed $\gamma > 0$. Then, we obtain the states near the intersection by volume averaging

$$\begin{aligned} h_1^\gamma &= \int_{-2\gamma}^{0} \int_{0}^{2\gamma} h^\gamma(x,y)\, dydx, \\ h_2^\gamma &= \int_{-\gamma}^{\gamma} \int_{-2\gamma}^{0} h^\gamma(x,y)\, dydx, \\ h_3^\gamma &= \int_{0}^{2\gamma} \int_{0}^{2\gamma} h^\gamma(x,y)\, dydx, \end{aligned} \tag{14}$$

and similarly for $(hu)_k^\gamma$, $k = 1, 2, 3$. Finally, we define boundary conditions for $h_k, (hu)_k$, $k = 1, 2, 3$ in the coupled one-dimensional model as limit of the previously obtained quantities when $\gamma \to 0$ *i.e.*,

$$\begin{aligned} h_1(b_1) &:= \lim_{\gamma \to 0} h_1^\gamma, \\ h_k(a_k) &:= \lim_{\gamma \to 0} h_k^\gamma, \qquad k = 2, 3, \end{aligned} \tag{15}$$

and analogously for $(hu)_1(b_1)$ and $(hu)_k(a_k)$ with $k = 2, 3$.

Remark 1. *Some remarks are in order:*

i. To simplify the computational effort in the considered method, one can also define boundary conditions for a fixed $\gamma > 0$.

ii. The previous discussion focused on constant initial data since we later on compare with the analytical results, see section 5. However, the approach is not limited to this case.

iii. The presentation has been given for a specific tee only, but is completely analogous in the other possible case of a tee intersection, as the right plot in Figure 3, or more general geometries.

iv. In the equations (12) we may also have friction terms. However, in the network model (4) canal fittings are considered as points of zero length. To obtain comparable numerical results we simulate (12) without friction effects, but we emphasize that the proposed approach is not limited to this case.

4.1. Numerical solution

The equations (12) can be solved using already existing software from computational fluid dynamics (CFD). Our focus in the present study is on investigating the coupling conditions described in the previous section rather than developing new numerical method for solving the partial differential equations (12). Therefore, we shall briefly highlight the schemes used for numerical solution of (12) and the main part of the present work is devoted to discuss the procedure used to verify the coupling conditions at canal junctions. Hence, the equations (12) are rearranged in a compact vector form as

$$\partial_t \mathbf{U} + \partial_x \mathbf{F}(\mathbf{U}) + \partial_y \mathbf{G}(\mathbf{U}) = \mathbf{0}, \tag{16}$$

where

$$\mathbf{U} = \begin{pmatrix} h \\ hu \\ hv \end{pmatrix}, \qquad \mathbf{F}(\mathbf{U}) = \begin{pmatrix} hu \\ hu^2 + p \\ huv \end{pmatrix}, \qquad \mathbf{G}(\mathbf{U}) = \begin{pmatrix} hv \\ huv \\ hv^2 + p \end{pmatrix}.$$

It is easy to verify that the system (16) is hyperbolic with distinct eigenvalues given by

$$\begin{aligned} \lambda^- &= u - \sqrt{gh}, \qquad \lambda^0 = u, \qquad \lambda^+ = u + \sqrt{gh}, \\ \mu^- &= v - \sqrt{gh}, \qquad \mu^0 = v, \qquad \mu^+ = u + \sqrt{gh}. \end{aligned} \tag{17}$$

To discretize the equations in space we consider, for simplicity in presentation, a uniform control volume $[x_{i-1/2}, x_{i+1/2}] \times [y_{j-1/2}, y_{j+1/2}]$ with mesh sizes $\Delta x = x_{i+1/2} - x_{i-1/2}$ and $\Delta y = y_{j+1/2} - y_{j-1/2}$ in x- and y-direction, respectively. Integrating (16) over the control volume and keeping the time continuous we obtain the following semi-discrete system

$$\frac{d\mathbf{U}_{i,j}}{dt} + \frac{\mathbf{F}\left(\mathbf{U}_{i+1/2,j}\right) - \mathbf{F}\left(\mathbf{U}_{i-1/2,j}\right)}{\Delta x} + \frac{\mathbf{G}\left(\mathbf{U}_{i,j+1/2}\right) - \mathbf{G}\left(\mathbf{U}_{i,j-1/2}\right)}{\Delta y} = \mathbf{0}, \tag{18}$$

where $\Psi_{i,j}$ is the space average of a generic function Ψ in the control volume $[x_{i-1/2}, x_{i+1/2}] \times [y_{j-1/2}, y_{j+1/2}]$ defined as

$$\Psi_{i,j} = \frac{1}{\Delta x}\frac{1}{\Delta y}\int_{x_{i-1/2}}^{x_{i+1/2}} \int_{y_{j-1/2}}^{y_{j+1/2}} \Psi(t,x,y)dxdy,$$

whereas, $\Psi_{i+1/2j} = \Psi(t, x_{i+1/2}, y_j)$ and $\Psi_{ij+1/2} = \Psi(t, x_i, y_{j+1/2})$ are the intermediate solutions used for numerical fluxes in (18) at $(x_{i+1/2}, y_j)$ and $(x_i, y_{j+1/2})$, respectively. The spatial discretization is complete when a numerical reconstruction of the fluxes in (18) is chosen.

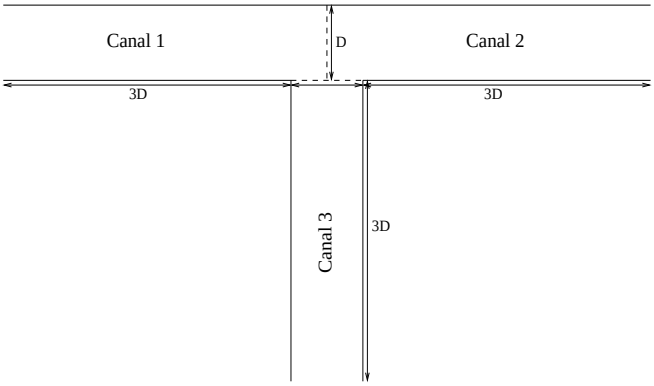

Figure 5. Spatial domain used for two-dimensional simulations.

Let the time interval $[0, T]$ be divided into subintervals $[t_n, t_{n+1}]$ of length Δt such that $t_n = n\Delta t$ and we use the notation $\Psi^n_{i,j} = \Psi_{i,j}(t_n)$. The procedure to advance the numerical solution of (18) from the time t_n to the next time t_{n+1} can be carried out as

$$\begin{aligned} \mathbf{U}^{(1)}_{i,j} &= \mathbf{U}^n_{i,j} + \Delta t \mathbf{R}\left(\mathbf{U}^n_{i,j}\right), \\ \mathbf{U}^{(2)}_{i,j} &= \frac{3}{4}\mathbf{U}^n_{i,j} + \frac{1}{4}\mathbf{U}^{(1)}_{i,j} + \frac{1}{4}\Delta t \mathbf{R}\left(\mathbf{U}^{(1)}_{i,j}\right), \\ \mathbf{U}^{n+1}_{i,j} &= \frac{1}{3}\mathbf{U}^n_{i,j} + \frac{2}{3}\mathbf{U}^{(2)}_{i,j} + \frac{2}{3}\Delta t \mathbf{R}\left(\mathbf{U}^{(2)}_{i,j}\right), \end{aligned} \tag{19}$$

where $\mathbf{R}$ stands for the right-hand side in (18) *i.e.*,

$$\mathbf{R}\left(\mathbf{U}_{i,j}\right) = -\frac{\mathbf{F}\left(\mathbf{U}_{i+1/2,j}\right) - \mathbf{F}\left(\mathbf{U}_{i-1/2,j}\right)}{\Delta x} - \frac{\mathbf{G}\left(\mathbf{U}_{i,j+1/2}\right) - \mathbf{G}\left(\mathbf{U}_{i,j-1/2}\right)}{\Delta y}.$$

This class of explicit time integration schemes has become popular in CFD algorithms, see for example [31, 19]. The scheme (19) is TVD, third-order accurate in time, and stable under the usual Courant-Friedrichs-Lewy (CFL) condition.

In order to reconstruct the numerical fluxes in the semi-discrete system (18), we consider a relaxation-based method. This method reconstructs the fluxes without relying on Riemann problem solvers and can be used with arbitrary order of accuracy. The first-order and second-order relaxation methods were first proposed in [23] to solve hyperbolic systems of conservation laws. A third-order relaxation scheme has also been proposed in [3] and intensively tested in [28, 29, 30] for a wide hyperbolic systems of conservation laws. The third-order method in the above mentioned references reconstructs the fluxes in (18) using linear combination of small stencils such that the overall combination preserves the third-order accuracy. In the present work, we formulate a fifth-order reconstruction for the numerical fluxes in (18). The key idea is to replace the linear weights in the third-order reconstruction by nonlinear weights capable of reducing the spurious oscillations that usually develop in regions with discontinuous derivatives. For the sake of completeness, the reconstruction of the numerical fluxes in (18) is detailed in the appendix.

4.2. Solution procedure

The numerical method described in the previous section is used to solve the two-dimensional shallow water equations (12) in the computational domain shown in Figure 5. Here, using the canal diameter D as a reference length, the domain is $4D$ high and $7D$ wide. Initial conditions are taken as

$$\begin{pmatrix} h(0,x,y) \\ \mathcal{P}(0,x,y) \\ \mathcal{Q}(0,x,y) \end{pmatrix} = \begin{cases} \begin{pmatrix} h_1 \\ \mathcal{P}_1 \\ 0 \end{pmatrix}, & \text{in Canal 1,} \\ \begin{pmatrix} h_2 \\ \mathcal{P}_2 \\ 0 \end{pmatrix}, & \text{in Canal 2,} \\ \begin{pmatrix} h_3 \\ 0 \\ \mathcal{Q}_3 \end{pmatrix}, & \text{in Canal 3,} \end{cases} \tag{20}$$

where the water discharges are

$$\mathcal{P} = h\,u \qquad \text{and} \qquad \mathcal{Q} = h\,v.$$

Other canal intersections can be handled in a similar manner. No-slip boundary conditions are imposed on the solid walls and homogeneous characteristic conditions are used for the open boundaries. The no-slip boundary condition is used to obtain a similar situation as in the one-dimensional test cases. The condition represents the fact that the velocity of the water is close to zero a the boundaries of the canals and is commonly used for viscous fluids. The characteristic speeds $A_{i+1/2,j}$ and $B_{i,j+1/2}$ in (33) and (34) can be chosen based on rough estimates of eigenvalues (17). Other choice is to calculate the characteristic speeds locally at each control volume $[x_{i-1/2}, x_{i+1/2}] \times [y_{j-1/2}, y_{j+1/2}]$ as

$$A_{i+1/2,j} = \max\Big\{ |\lambda^L_{i+1/2,j}|, |\lambda^R_{i+1/2,j}| \Big\}, \qquad B_{i,j+1/2} = \max\Big\{ |\mu^L_{i,j+1/2}|, |\mu^R_{i,j+1/2}| \Big\}, \tag{21}$$

where λ and μ are the eigenvalues (17) approximated according to (30). It should be stressed that larger values of $A_{i+1/2,j}$ and $B_{i,j+1/2}$ usually add more numerical dissipation to the relaxation scheme.

The aim of the presented simulations is to verify the coupling conditions which are commonly imposed in many engineering applications. We simulate different inflow configurations for two types of tee intersections with three connected canals. We stop the two-dimensional simulation whenever a wave exists the computational domain. This corresponds to the analytical discussion where only waves of negative (respectively positive) speed emerge from the canal-to-canal intersection. In the second stage, we average the computed results to obtain equivalent one-dimensional fluxes and pressures for each canal (referred to as simulation results in the sequel) and compare these values with the analytical results obtained in [5]. Due to additional geometry effects in the two-dimensional simulation we do not expect a full

coincidence in the analytical and simulation results. But we are looking for a verification of the underlying principle of conservation of mass and equal water head or water pressure at the tee intersections. Furthermore, we expect both the analytical and simulation results to behave in a similar way when changing the initial conditions.

5. NUMERICAL RESULTS

In this section we examine the accuracy of the proposed method for several different situations and verify the coupling conditions at junctions in canal networks. We test the ability of our scheme to verify the coupling conditions for two types of junctions in a canal network. All the results presented in this section are obtained using the local characteristic speeds (21) and a variable time step adjusted according to the stability condition

$$\Delta t = \mathrm{Cr} \min \left(\frac{\Delta x}{\left| A^2_{i+1/2,j} \right|}, \frac{\Delta y}{\left| B^2_{i,j+1/2} \right|} \right), \tag{22}$$

where the Courant number Cr is fixed to 0.8. This section is devoted to numerically verify the coupling conditions described in the present work. In the sequel, we consider the two types of tee fittings illustrated in Figure 3, namely, one canal with ingoing water flow and two canals with outgoing water flow (referred to as 1-to-2 situation) for the first example. For the second example, two canals with ingoing water flow and one canal with outgoing flow (referred to as 2-to-1 situation) are considered. Except otherwise stated, the canal diameter is fixed to $D = 0.5$ in all our computations and the parameter $\gamma = D$ in the equations (13) and (14).

5.1. Grid dependence study

In this section we examine the grid effects on the computed two-dimensional solutions. To this end we consider the 1-to-2 situation subject to the following initial conditions:

$$\begin{pmatrix} h^0(x,y) \\ (hu)^0(x,y) \\ (hv)^0(x,y) \end{pmatrix} = \begin{cases} \begin{pmatrix} 1.3 \\ 0 \\ 0 \end{pmatrix}, & \text{if} \quad (x,y) \in]-\infty, 0[\times]0, 2\gamma[, \\ \begin{pmatrix} 1 \\ 0 \\ 0 \end{pmatrix}, & \text{if} \quad (x,y) \in]0, \infty[\times]0, 2\gamma[, \\ \begin{pmatrix} 1 \\ 0 \\ 0 \end{pmatrix}, & \text{if} \quad (x,y) \in]-\gamma, \gamma[\times]-\infty, 0[. \end{cases} \tag{23}$$

In the first runs for this test example we consider a series of uniform meshes with $\Delta x = \Delta y$. In Figure 6 we show the grid effects on profiles of water height and velocity field at the mid-width

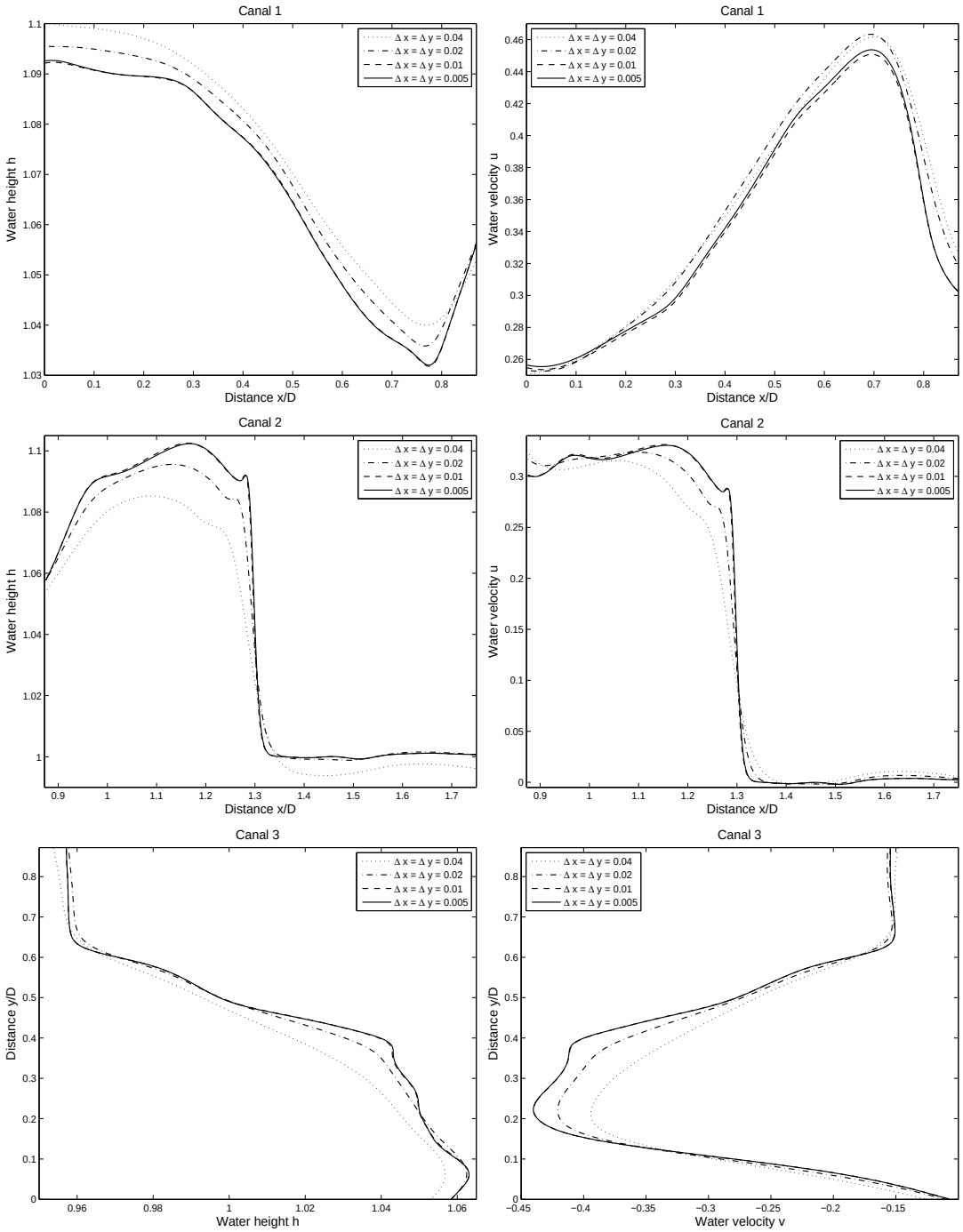

Figure 6. Cross sections of water height (left) and water velocity (right) for the 1-to-2 situation at time $t = 0.25$ using four different meshes.

of each canal at time $t = 0.25$ using four different meshes with $\Delta x = \Delta y = 0.04$, 0.02, 0.01 and 0.005. It is easy to see that solutions obtained using the mesh with $\Delta x = \Delta y = 0.04$ are far from those obtained by the other meshes. Decreasing the spatial stepsize, results for the mesh with $\Delta x = \Delta y = 0.01$ and the mesh with $\Delta x = \Delta y = 0.005$ are roughly similar. As can be observed, there is little differences between the last two mesh levels. For instance, we have found that the discrepancies in the maximum and minimum values of the water height and the water velocity on the mesh $\Delta x = \Delta y = 0.02$ and the mesh $\Delta x = \Delta y = 0.005$ are less than 7%. These differences become less than 0.2% on the mesh $\Delta x = \Delta y = 0.01$ and the mesh $\Delta x = \Delta y = 0.005$. Similar behavior has been observed for the results, not reported here, for the 2-to-1 situation. These results ensure grid independence of the numerical results. Therefore, bearing in mind the slight change in the results from the mesh with $\Delta x = \Delta y = 0.01$ and the mesh with $\Delta x = \Delta y = 0.005$ at the expense of rather significant increase in the computational cost, the mesh with $\Delta x = \Delta y = 0.01$ is believed to be adequate to obtain the results free of grid effects. Hence, the results presented herein are based on the mesh with $\Delta x = \Delta y = 0.01$.

5.2. Verification of coupling conditions

We first consider the two-dimensional dynamics in the 1-to-2 situation. Figure 7 illustrates the water height at four different times $t = 0.1$, 0.25, 0.5 and 1 using the initial conditions (23). The associated flow fields are presented in Figure 8. As can be seen from these results, the water flow enters the first canal and generates a moving shock and a rarefaction wave. Once it reaches the junction, the water is distributed in the two outflowing canals. Small recirculation zones can also be observed in the flow field in the upper and backward walls. At the final time, the water flow exhibits a steady-state pattern. It is evident that our high-order relaxation-based scheme captures accurately the evolution of the interface in the computational domain without diffusing the fronts or introducing oscillations near steep gradients. To further demonstrate the flow dynamics, we plot in Figure 9 the time evolution of the volume averaging for the flow variables using the procedure (14) in the tee intersection. Here we show the time evolution of the volume averaging for the water height, water pressure, water head and water discharge. For the considered flow conditions, only the water height, water pressure and water head at each canal seem to converge to the same values for long time simulation. A huge discrepancy is detected for the volume averaging of the water discharge at each canal. It should be stressed that similar flow trends have been observed for numerical results, not included here, for the 2-to-1 situation.

Next we turn to the comparison of analytical and numerical results for the averaged flow variables as explained in Section 3 for different initial conditions. We give analytical results for the 1-to-2 situation in Table I and our two-dimensional numerical results in the lower part of Table I. The initial data in canal two and three is as in equation (23). In canal one we use the values (h, Q) of Table I *i.e.*, we prescribe for the two-dimensional simulations

$$\begin{pmatrix} h^0(x,y) \\ (hu)^0(x,y) \\ (hv)^0(x,y) \end{pmatrix} = \begin{pmatrix} h \\ Q \\ 0 \end{pmatrix}, \qquad \forall\, (x,y) \in]-\infty, 0[\times]0, 2\gamma[.$$

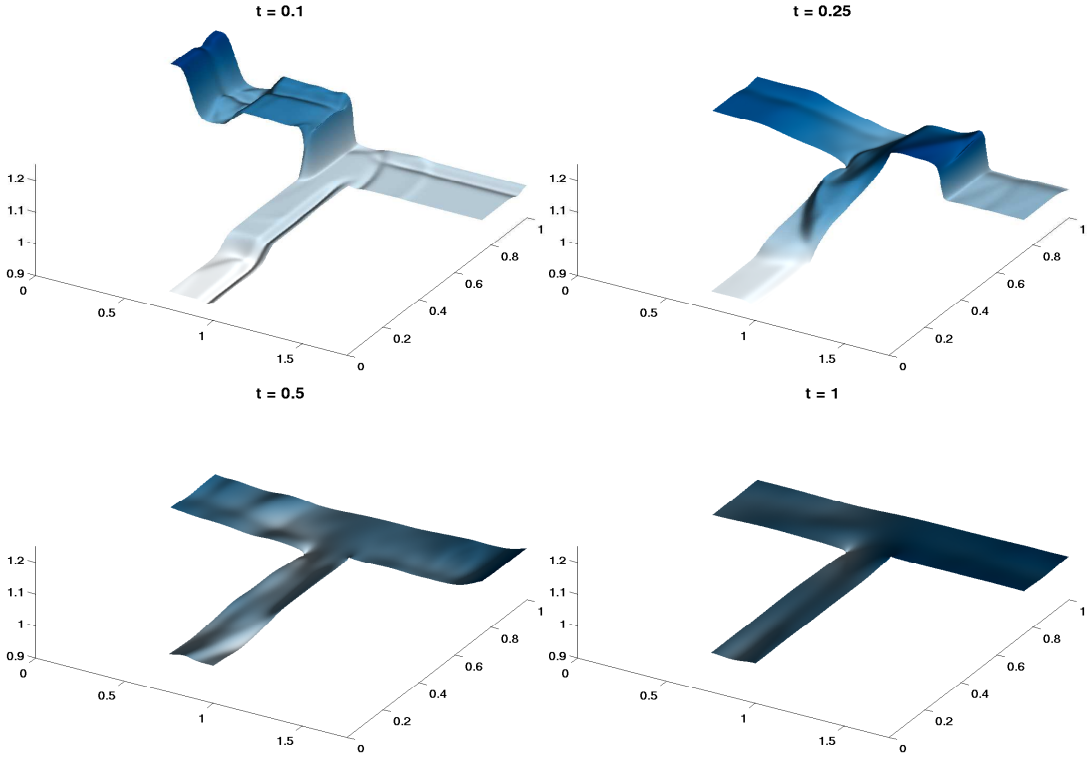

Figure 7. Water free-surface for the 1-to-2 situation at four different times.

For all perturbations, the equal head condition does produce slightly higher water heads at the node which is justified by the numerical situations. The predicted heads and pressures show a similar trend for all perturbations. The values for water head differ possibly due to additional geometric effects up to 60% for strong perturbations and about 40% for small perturbations. The prediction for the water height are more reliable and they differ by only up to 10% compared with the equal head condition. We observe that in case of strong perturbations the water discharge Q is not correctly predicted by both the equal pressure and the equal head conditions. The values for the water discharge in the numerical simulation are very small and therefore the sign of the discharge is not reliable. Since the water height is correctly predicted we conclude that the velocity distribution in the two-dimensional situation does not allow for a simple average procedure to obtain the one-dimensional velocity fields.

Our next concern is to verify the coupling conditions for the 2-to-1 situation. As in the previous situation we display in Figure 10 the water height at four different times $t = 0.1$, 0.25, 0.5 and 1. The corresponding flow fields are presented in Figure 11. In contrast to the previous situation, the water flow in this case enters the tee intersection from two canals generating a strong and weak shocks at the junction. The initial condition in canal one and

Table I. Analytical results for coupling conditions at the junction in the 1–to–2 junction. Here, the terminal values at the node are listed at time $t = 1$ in the different canals. We display the conservation of mass condition (6) and the additional condition as indicated and numerical results, respectively. Initial values in canal one are given in the first column.

Equal pressure at the junction (7)

Perturb canal 1		Water height h			Water pressure p			Water head H			Water discharge Q		
h	Q	Canal 1	Canal 2	Canal 3	Canal 1	Canal 2	Canal 3	Canal 1	Canal 2	Canal 3	Canal 1	Canal 2	Canal 3
+0.500	-0.9261	+0.6473	+0.6473	+0.6473	+2.0948	+2.0948	+2.0948	+0.9529	+0.7237	+0.7237	-1.6004	-0.8002	-0.8002
+0.700	-0.7232	+0.7940	+0.7940	+0.7940	+3.1524	+3.1524	+3.1524	+0.8889	+0.8178	+0.8178	-1.0940	-0.5470	-0.5470
+0.900	-0.2921	+0.9327	+0.9327	+0.9327	+4.3501	+4.3501	+4.3501	+0.9421	+0.9351	+0.9351	-0.4036	-0.2018	-0.2018
+1.100	+0.3399	+1.0661	+1.0661	+1.0661	+5.6834	+5.6834	+5.6834	+1.0746	+1.0683	+1.0683	+0.4391	+0.2195	+0.2195
+1.300	+1.1600	+1.1959	+1.1959	+1.1959	+7.1507	+7.1507	+7.1507	+1.2663	+1.2135	+1.2135	+1.4196	+0.7098	+0.7098
+1.500	+2.1630	+1.3231	+1.3231	+1.3231	+8.7527	+8.7527	+8.7527	+1.5063	+1.3689	+1.3689	+2.5331	+1.2665	+1.2665

Equal head at the junction (8)

Perturb canal 1		Water height h			Water pressure p			Water head H			Water discharge Q		
h	Q	Canal 1	Canal 2	Canal 3	Canal 1	Canal 2	Canal 3	Canal 1	Canal 2	Canal 3	Canal 1	Canal 2	Canal 3
+0.500	-0.9261	+0.5668	+0.7647	+0.7647	+1.6062	+2.9240	+2.9240	+0.7962	+0.7962	+0.7962	-1.2141	-0.6071	-0.6071
+0.700	-0.7232	+0.7616	+0.8242	+0.8242	+2.9005	+3.3965	+3.3965	+0.8412	+0.8412	+0.8412	-0.9606	-0.4803	-0.4803
+0.900	-0.2921	+0.9286	+0.9353	+0.9353	+4.3118	+4.3736	+4.3736	+0.9374	+0.9374	+0.9374	-0.3894	-0.1947	-0.1947
+1.100	+0.3399	+1.0613	+1.0681	+1.0681	+5.6316	+5.7046	+5.7046	+1.0704	+1.0704	+1.0704	+0.4529	+0.2265	+0.2265
+1.300	+1.1600	+1.1394	+1.2106	+1.2106	+6.4915	+7.3279	+7.3279	+1.2309	+1.2309	+1.2309	+1.5408	+0.7704	+0.7704
+1.500	+2.1630	+1.0210	+1.3572	+1.3572	+5.2118	+9.2103	+9.2103	+1.4126	+1.4126	+1.4126	+2.8575	+1.4288	+1.4288

Numerical results obtained by averaging at time $t = 1$

Perturb canal 1		Water height h			Water pressure p			Water head H			Water discharge Q		
h	Q	Canal 1	Canal 2	Canal 3	Canal 1	Canal 2	Canal 3	Canal 1	Canal 2	Canal 3	Canal 1	Canal 2	Canal 3
+0.500	-0.9261	+0.5100	+0.5102	+0.5101	+1.3005	+1.3017	+1.3012	+0.5102	+1.0207	+1.0211	-0.0337	-0.0081	-0.0156
+0.700	-0.7232	+0.8222	+0.8222	+0.8221	+3.3805	+3.3800	+3.3794	+0.8222	+1.6444	+1.6442	+0.00394	+0.0099	+0.0005
+0.900	-0.2921	+0.9261	+0.9261	+0.9261	+4.2890	+4.2886	+4.2884	+0.9261	+1.8522	+1.8522	+0.0001	+0.0031	-0.0000
+1.100	+0.3399	+1.0094	+1.0094	+1.0094	+5.0948	+5.0948	+5.0953	+1.0094	+2.0188	+2.0189	-0.0013	-0.0035	-0.0001
+1.300	+1.1600	+1.1171	+1.1171	+1.1170	+6.2395	+6.2397	+6.2394	+1.1171	+2.2342	+2.2341	-0.0034	+0.0013	-0.0005
+1.500	+2.1630	+1.2074	+1.2074	+1.2074	+7.2891	+7.2891	+7.2890	+1.2074	+2.4148	+2.4148	-0.0030	+0.0038	-0.0005

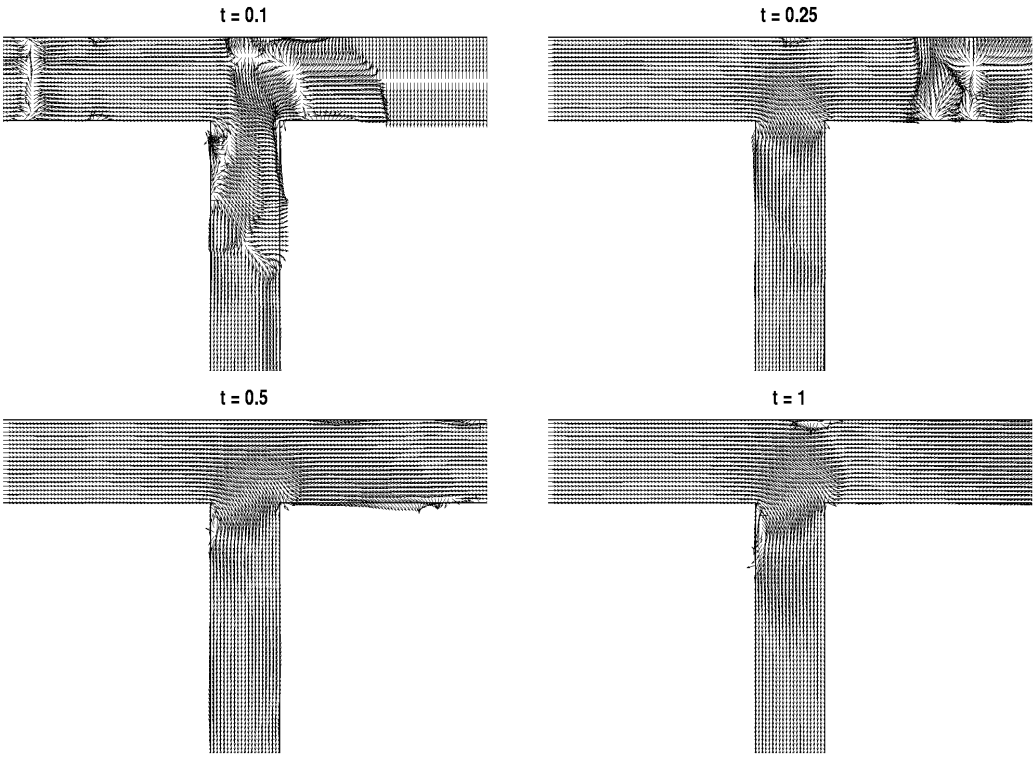

Figure 8. Velocity field (u, v) for the 1-to-2 situation at four different times.

three are given by the values of (h, Q) of the first column in Table II. We have

$$\begin{pmatrix} h^0(x,y) \\ (hu)^0(x,y) \\ (hv)^0(x,y) \end{pmatrix} = \begin{cases} \begin{pmatrix} h \\ Q \\ 0 \end{pmatrix}, & \forall\ (x,y) \in]-\infty, 0[\times]0, 2\gamma[, \\ \\ \begin{pmatrix} h \\ 0 \\ Q \end{pmatrix}, & \forall\ (x,y) \in]-\gamma, \gamma[\times]-\infty, 0[. \end{cases} \tag{24}$$

Again, at the final simulation time the water system stabilizes to an equilibrium state. As can be seen, the proposed relaxation method accurately solves this flow problem and captures the correct water flow features. We should mention that the performance of the relaxation method is very attractive since the computed solution remains stable and accurate even when coarse meshes are used without requiring complicated Riemann problem solvers.

We now consider varying initial data and check for qualitative agreement between numerical and theoretical results. Hence, the obtained results for the 2-to-1 situation are discussed in

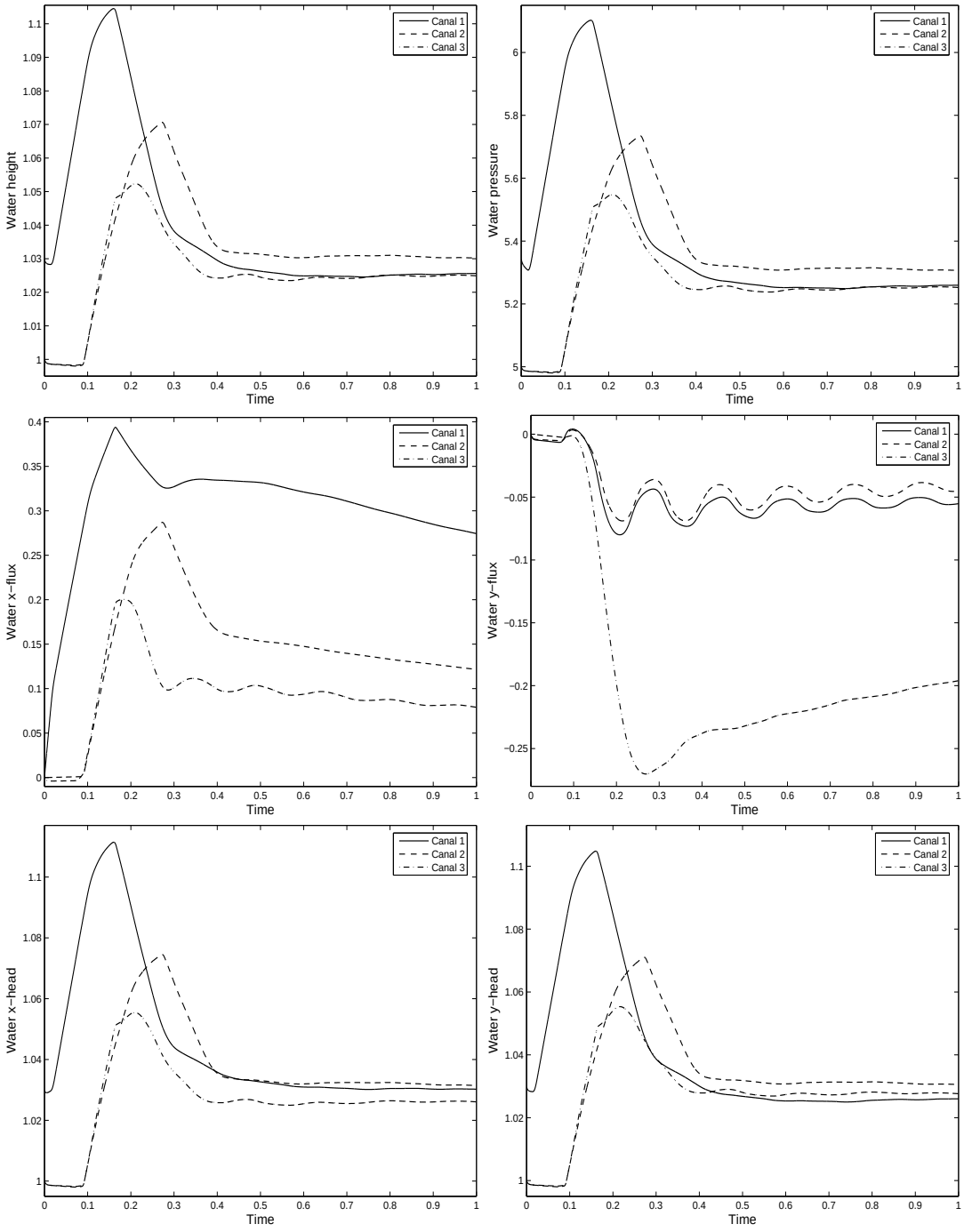

Figure 9. Time evolution of the volume averaging for the water flow components at each canal.

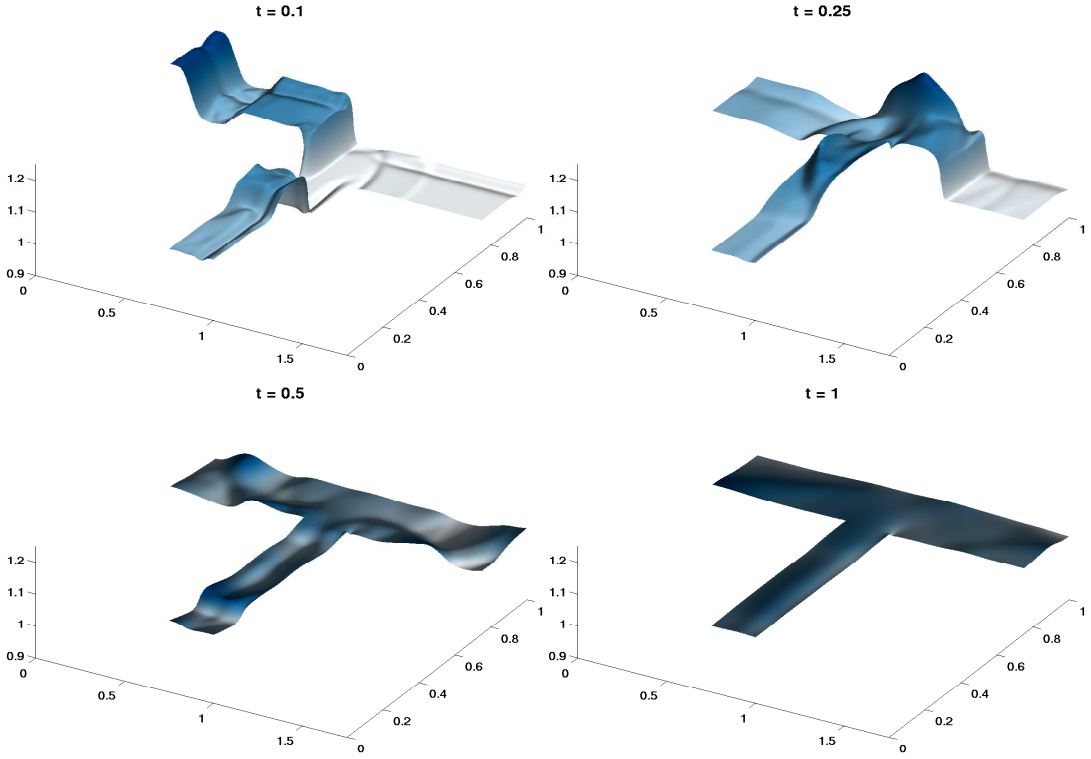

Figure 10. Water free-surface for the 2-to-1 situation at four different times.

Table II for the analytically computed coupling conditions and also for the numerical values. Here, we observe similar effects as in the previous 1–to–2 situation. The prediction of the water discharge is not correct and the absolute values as well as the trend differs between numerical and analytical study. Since the prediction of the water height is within a similar range than for the 1-to-2 situation, this again suggests that the velocity profile within the intersection is very different to a one-dimensional approach.

Summarizing, in both situations we observe a mismatch of predicted water velocity profiles. The following reasons might lead to these results. Most likely geometry effects have to be included in the one-dimensional model by either modified conditions at the junction or by replacing the coupling conditions with the above given tables. The study of perturbations of a steady-state solution is more realistic in terms of applications but the strength of realistic perturbations remain unclear. Even so the water discharge is not predicted well for the considered flow cases and therefore, there is still some values in the one-dimensional simulations due to the good forecast of water heights which allow *e.g.*, to conduct flooding predictions.

Our final concern is to check the influence of the canal dimensions on the obtained numerical results. To this end we perform numerical simulations with varying the length and the diameter of the canal in the 1–to–2 situation. Table III presents results for simulations obtained for canal

Table II. Analytical results for coupling conditions at the junction in the 2–to–1 junction. Here, the terminal values at the node are listed at time $t = 1$ in the different canals. We display the conservation of mass condition (6) and the additional condition as indicated and numerical results, respectively. Initial values in canal one are given in the first column.

Equal pressure at the junction (7)

Perturb canal 1		Water height h			Water pressure p			Water head H			Water discharge Q		
h	Q	Canal 1	Canal 2	Canal 3	Canal 1	Canal 2	Canal 3	Canal 1	Canal 2	Canal 3	Canal 1	Canal 2	Canal 3
+0.500	-0.9261	+0.3715	+0.3715	+0.3715	+0.6899	+0.6899	+0.6899	+0.4477	+0.6765	+0.4477	-0.4587	-0.9175	-0.4587
+0.600	-0.8554	+0.4892	+0.4892	+0.4892	+1.1968	+1.1968	+1.1968	+0.5344	+0.6699	+0.5344	-0.4650	-0.9299	-0.4650
+0.700	-0.7232	+0.6119	+0.6119	+0.6119	+1.8718	+1.8718	+1.8718	+0.6356	+0.7067	+0.6356	-0.4214	-0.8428	-0.4214
+0.800	-0.5342	+0.7383	+0.7383	+0.7383	+2.7253	+2.7253	+2.7253	+0.7482	+0.7779	+0.7482	-0.3286	-0.6573	-0.3286

Numerical results obtained by averaging at time $t = 1$

Perturb canal 1		Water height h			Water pressure p			Water head $\mathcal{H}$			Water discharge Q		
h	Q	Canal 1	Canal 2	Canal 3	Canal 1	Canal 2	Canal 3	Canal 1	Canal 2	Canal 3	Canal 1	Canal 2	Canal 3
+0.500	-0.9261	+0.1797	+0.1797	+0.1708	+0.1616	+0.1616	+0.1462	+0.1805	+0.3618	+0.3503	+0.0073	-0.0317	+0.0003
+0.600	-0.8554	+0.3858	+0.3859	+0.3855	+0.7444	+0.7446	+0.7432	+0.3859	+0.7720	+0.7718	+0.0079	-0.0177	+0.0018
+0.700	-0.7232	+0.5837	+0.5837	+0.5838	+1.7038	+1.7040	+1.7043	+0.5837	1.1676	1.1677	+0.0061	-0.0036	+0.0008
+0.800	-0.5342	+0.7328	+0.7328	+0.7328	+2.6851	+2.6852	+2.6853	+0.7328	+1.4657	1.4657	+0.0034	+0.0000	+0.0002

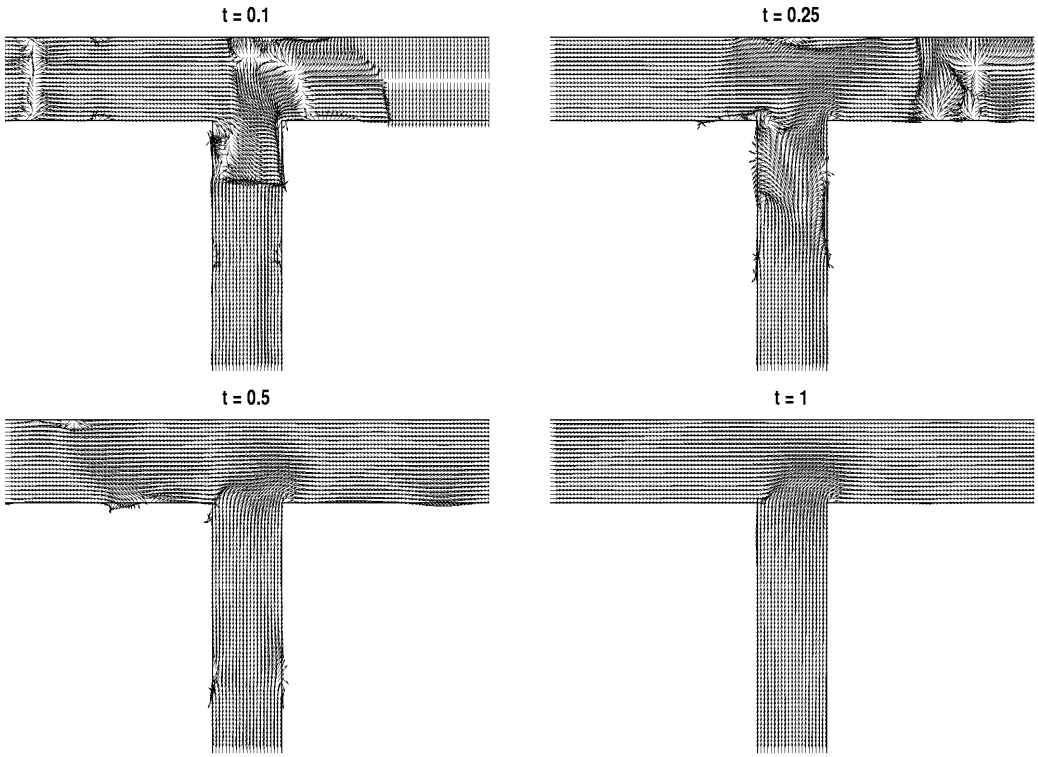

Figure 11. Velocity field for the 2-to-1 situation at four different times.

diameter $D = 0.25$, 0.5 and 0.75. The length of the canal is chosen such that the total area is constant. Note that the terminal time is set to $t = 1$ in all cases and no scaling has been included in the perturbations. As in the previous simulations, water height, pressure, head and discharge are obtained by averaging for each test case. These computed water variables are summarized in Table III. It is evident from the presented results that the canal dimensions do affect the simulated results for all considered cases. For instance, we have observed that there is a strong dependence on the specific layout of the canal of the terminal values. In particular for the canal with largest diameter neither water pressure nor water head are equal at the node. Among the possible reasons for these detected discrepancies are the fact that the computed solutions need more time to evolve.

6. SUMMARY

We have presented a method to compute coupling conditions in T-junction for water way or canal intersections. The governing equations are based on the canonical shallow water equations for open channel flows. The method is based on a local refined view on the dynamics close

Table III. Numerical results for coupling conditions at the junction in the 1–to–2 junction using different canal diameter and lengths. Here (1), (2) and (3) are numerical results obtained for canals with diameter $D = 0.25$ and length $9D$, diameter $D = 0.5$ and length $4.5D$, and diameter $D = 0.75$ and length $3D$, respectively

Perturb canal 1			Water height h			Water pressure p			Water head H			Water discharge Q		
h	Q		Canal 1	Canal 2	Canal 3	Canal 1	Canal 2	Canal 3	Canal 1	Canal 2	Canal 3	Canal 1	Canal 2	Canal 3
+0.5000	-0.9261	(1)	+0.5356	+0.5245	+0.5303	+1.3221	+1.3210	+1.3233	+0.5354	+1.0256	+1.0251	-0.0365	-0.0089	-0.0177
		(2)	+0.5100	+0.5102	+0.5101	+1.3005	+1.3017	+1.3012	+0.5102	+1.0207	+1.0211	-0.0337	-0.0081	-0.0156
		(3)	+0.6069	+0.9796	+0.9947	+1.5346	+2.4862	+2.5113	+0.6082	+1.9700	+1.9605	-0.0402	-0.0155	-0.0300
+0.700	-0.7232	(1)	+0.8301	+0.8302	+0.8301	+3.3985	+3.3979	+3.3903	+0.8301	+1.6507	+1.6600	+0.0045	+0.0101	+0.0006
		(2)	+0.8222	+0.8222	+0.8221	+3.3805	+3.3800	+3.3794	+0.8222	+1.6444	+1.6442	+0.0039	+0.0099	+0.0005
		(3)	+0.1603	+1.5868	+1.5702	+6.4906	+6.4896	+6.5053	+1.5786	+3.1737	+3.1569	+0.0074	+0.0192	+0.0009
+0.900	-0.2921	(1)	+0.9277	+0.9277	+0.9277	+4.2898	+4.2891	+4.2890	+0.9277	+1.8565	+1.8565	+0.0002	+0.0035	-0.0000
		(2)	+0.9261	+0.9261	+0.9261	+4.2890	+4.2886	+4.2884	+0.9261	+1.8522	+1.8522	+0.0001	+0.0031	-0.0000
		(3)	+1.7874	+1.7781	+1.7994	+8.1920	+8.1483	+8.2852	+1.7781	+3.5747	+3.5859	+0.0003	+0.0060	-0.0001
+1.100	+0.3399	(1)	+1.0098	+1.0098	+1.0098	+5.0971	+5.0972	+5.0969	+1.0098	+2.0197	+2.0198	-0.0015	-0.0037	-0.0002
		(2)	+1.0094	+1.0094	+1.0094	+5.0948	+5.0948	+5.0953	+1.0094	+2.0188	+2.0189	-0.0013	-0.0035	-0.0001
		(3)	+1.9481	+1.9683	+1.9615	+9.6801	+9.7056	+9.7881	+1.9280	+3.8963	+3.9050	-0.0025	-0.0067	-0.0003
+1.300	+1.1600	(1)	+1.1187	+1.1187	+1.1187	+6.2399	+6.2399	+6.2399	+1.1187	+2.2355	+2.2355	-0.0037	+0.0019	-0.0006
		(2)	+1.1171	+1.1171	+1.1170	+6.2395	+6.2397	+6.2394	+1.1171	+2.2342	+2.2341	-0.0034	+0.0013	-0.0005
		(3)	+2.1783	+2.1560	+2.1582	+11.7927	+11.7244	+11.8361	+2.1672	+4.3567	+4.3453	-0.0065	+0.0025	-0.0009
+1.500	+2.1630	(1)	+1.2083	+1.2083	+1.2083	+7.2899	+7.2899	+7.2897	+1.2083	+2.4157	+2.4157	-0.0034	+0.0040	-0.0006
		(2)	+1.2074	+1.2074	+1.2074	+7.2891	+7.2891	+7.2890	+1.2074	+2.4148	+2.4148	-0.0030	+0.0038	-0.0005
		(3)	+2.3424	+2.3061	+2.3462	+13.6306	+13.5577	+13.6698	+2.3182	+4.6847	+4.6383	-0.0059	+0.0073	-0.0010

to the canal-to-canal intersection point. There a two-dimensional formulation of the shallow water equations have been numerically discretized and solved using a high-order relaxation method. The proposed method replaces the nonlinear shallow water equations by a semi-linear hyperbolic system with linear characteristic speeds and easy to solve without relying on Riemann problem solvers or characteristic decomposition. The presented results show good shock resolution with high accuracy in smooth regions and without any non-physical oscillations near the shock areas. The numerical method has been used for verification and comparison with the theoretical results. Verifications are conducted for two types of junctions namely the 1-to-2 and 2-to-1 situations. For small perturbations of steady-state flow the numerically obtained results have been compared with the equal pressure and equal head conditions. Depending on the strength of the perturbation good agreement in the water height predictions could be observed. The averaged water velocity profiles however do not agree with the one-dimensional computation possibly due to the strong influence of the geometry.

Future work will concentrate on simulation of water flow in large networks such as irrigation systems. For example, using the coupling conditions summarized in the tables reported in this study, the resolution in the one-dimensional flow system may be improved.

APPENDIX

Associated with the equations (16) a relaxation approximation is

$$\begin{aligned} \partial_t \mathbf{U} + \partial_x \mathbf{V} + \partial_y \mathbf{W} &= \mathbf{0}, \\ \partial_t \mathbf{V} + \mathbf{A}^2 \partial_x \mathbf{U} &= -\frac{1}{\varepsilon}\left(\mathbf{V} - \mathbf{F}(\mathbf{U})\right), \\ \partial_t \mathbf{W} + \mathbf{B}^2 \partial_y \mathbf{U} &= -\frac{1}{\varepsilon}\left(\mathbf{W} - \mathbf{G}(\mathbf{U})\right), \end{aligned} \tag{25}$$

where $\mathbf{V} \in \mathbb{R}^3$ and $\mathbf{W} \in \mathbb{R}^3$ are relaxation variables, $\mathbf{A}^2$ and $\mathbf{B}^2$ are diagonal matrices in $\mathbb{R}^3 \times \mathbb{R}^3$ where their entries A_l^2 and B_l^2 are characteristic speeds of (16). The relaxation system (25) has a typical semi-linear structure with linear characteristic variables defined by

$$\mathcal{F}^{\pm} = \mathbf{V} \pm \mathbf{A}\mathbf{U} \qquad \text{and} \qquad \mathcal{G}^{\pm} = \mathbf{W} \pm \mathbf{B}\mathbf{U}. \tag{26}$$

Formally, in the zero relaxation limit $\varepsilon \longrightarrow 0$, we recover the original system (16) provided the subcharacteristic condition [23],

$$\frac{|\mathbf{F}_l'(\mathbf{U})|}{\mathbf{A}_l} + \frac{|\mathbf{G}_l'(\mathbf{U})|}{\mathbf{B}_l} \leq 1, \qquad \forall\, l = 1, 2, 3, \tag{27}$$

holds in (25). It is easy to verify that if we project the relaxation variables into the local equilibrium

$$\mathbf{V} = \mathbf{F}(\mathbf{U}) \qquad \text{and} \qquad \mathbf{W} = \mathbf{G}(\mathbf{U}), \tag{28}$$

then the first equation in (25) reduces to the original conservation laws (16). From a numerical view point, it is simpler to solve the system (25) than the original equations (16). Here, our fifth-order reconstruction is applicable directly to the linear characteristic variables (26). In

what follows we only formulate $\mathbf{U}_{i+1/2,j}$ and $\mathbf{V}_{i+1/2,j}$, and expressions for other fluxes are obtained in an entirely analogous manner.

Since the variables $\mathcal{F}^+$ and $\mathcal{F}^-$ travel respectively, along constant characteristics with speeds $+A$ and $-A$, a WENO reconstruction can be easily applied to them. Thus, the numerical fluxes $\mathcal{F}^{\pm}_{i+1/2,j}$ at the cell boundary $(x_{i+1/2}, y_j)$ are defined as left and right extrapolated values $\mathcal{F}^{+,L}_{i+1/2,j}$ and $\mathcal{F}^{-,R}_{i+1/2,j}$ by

$$\mathcal{F}^{+}_{i+1/2,j} = \mathcal{F}^{+,L}_{i+1/2,j}, \qquad \mathcal{F}^{-}_{i+1/2,j} = \mathcal{F}^{-,R}_{i+1/2,j}. \tag{29}$$

These extrapolated values are obtained from cell averages by means of high-order WENO polynomial reconstruction. Here, we use the fifth-order WENO reconstruction proposed in [22]. Higher-order reconstructions are also possible, such as those developed in [2]. For a generic function $\Psi(x, y)$ the fifth-order accurate left boundary extrapolated value $\Psi^{L}_{i+1/2,j}$ is defined as

$$\Psi^{L}_{i+1/2,j} = \omega_0 \mathcal{V}_0 + \omega_1 \mathcal{V}_1 + \omega_2 \mathcal{V}_2, \tag{30}$$

where $\mathcal{V}_r$ is the extrapolated value obtained from cell averages in the rth stencil $(i-r, i-r+1, i-r+2)$ in x-direction

$$\begin{aligned}
\mathcal{V}_0 &= \frac{1}{6}\left(-\Psi_{i+2,j} + 5\Psi_{i+1,j} + 2\Psi_{i,j}\right), \\
\mathcal{V}_1 &= \frac{1}{6}\left(-\Psi_{i-1,j} + 5\Psi_{i,j} + 2\Psi_{i+1,j}\right), \\
\mathcal{V}_2 &= \frac{1}{6}\left(2\Psi_{i-2,j} - 7\Psi_{i-1,j} + 11\Psi_{i,j}\right),
\end{aligned}$$

and ω_r, $r = 0, 1, 2$, are nonlinear WENO weights given by

$$\omega_k = \frac{\alpha_k}{\sum_{l=0}^{2} \alpha_l}, \qquad \alpha_0 = \frac{3}{10(\tau + IS_0)^2}, \qquad \alpha_1 = \frac{3}{5(\tau + IS_1)^2}, \qquad \alpha_2 = \frac{1}{10(\tau + IS_2)^2}. \tag{31}$$

Here the parameter τ is introduced to guarantee that the denominator does not vanish and is empirically taken to be 10^{-6}. The smoothness indicators IS_r, $r = 0, 1, 2$, are given by [22]

$$\begin{aligned}
IS_0 &= \frac{13}{12}\left(\Psi_{i,j} - 2\Psi_{i+1,j} + \Psi_{i+2,j}\right)^2 + \frac{1}{4}\left(3\Psi_{i,j} - 4\Psi_{i+1,j} + \Psi_{i+2,j}\right)^2, \\
IS_1 &= \frac{13}{12}\left(\Psi_{i-1,j} - 2\Psi_{i,j} + \Psi_{i+1,j}\right)^2 + \frac{1}{4}\left(\Psi_{i-1,j} - \Psi_{i+1,j}\right)^2, \\
IS_2 &= \frac{13}{12}\left(\Psi_{i-2,j} - 2\Psi_{i-1,j} + \Psi_{i,j}\right)^2 + \frac{1}{4}\left(\Psi_{i-2,j} - 4\Psi_{i-1,j} + 3\Psi_{i,j}\right)^2.
\end{aligned}$$

The right value $\Psi^{R}_{i+1/2,j}$ is obtained by symmetry as

$$\Psi^{R}_{i+1/2,j} = \omega_0 \mathcal{V}_0 + \omega_1 \mathcal{V}_1 + \omega_2 \mathcal{V}_2, \tag{32}$$

where

$$\begin{aligned}
\mathcal{V}_0 &= \frac{1}{6}\left(2\Psi_{i+3,j} - 7\Psi_{i+2,j} + 11\Psi_{i+1,j}\right), \\
\mathcal{V}_1 &= \frac{1}{6}\left(-\Psi_{i+2,j} + 5\Psi_{i+1,j} + 2\Psi_{i,j}\right), \\
\mathcal{V}_2 &= \frac{1}{6}\left(-\Psi_{i-1,j} + 5\Psi_{i,j} + 2\Psi_{i+1,j}\right).
\end{aligned}$$

The corresponding weights and smoothness indicators are given by (31) with

$$\begin{aligned} IS_0 &= \frac{13}{12}\left(\Psi_{i+1,j} - 2\Psi_{i+2,j} + \Psi_{i+3,j}\right)^2 + \frac{1}{4}\left(3\Psi_{i+1,j} - 4\Psi_{i+2,j} + \Psi_{i+3,j}\right)^2, \\ IS_1 &= \frac{13}{12}\left(\Psi_{i,j} - 2\Psi_{i+1,j} + \Psi_{i+2,j}\right)^2 + \frac{1}{4}\left(\Psi_{i,j} - \Psi_{i+2,j}\right)^2, \\ IS_2 &= \frac{13}{12}\left(\Psi_{i-1,j} - 2\Psi_{i,j} + \Psi_{i+1,j}\right)^2 + \frac{1}{4}\left(\Psi_{i-1,j} - 4\Psi_{i,j} + 3\Psi_{i+1,j}\right)^2. \end{aligned}$$

Once $\mathcal{F}^+_{i+1/2,j}$ and $\mathcal{F}^-_{i+1/2,j}$ are reconstructed in (29), the numerical fluxes $\mathbf{U}_{i+1/2,j}$ and $\mathbf{V}_{i+1/2,j}$ in the relaxation system are obtained from (26) by

$$\mathbf{U}_{i+1/2,j} = \frac{1}{2A_{i+1/2,j}}\left(\mathcal{F}^+_{i+1/2,j} - \mathcal{F}^-_{i+1/2,j}\right), \qquad \mathbf{V}_{i+1/2,j} = \frac{1}{2}\left(\mathcal{F}^+_{i+1/2,j} + \mathcal{F}^-_{i+1/2,j}\right). \quad (33)$$

Analogously, the numerical fluxes $\mathbf{U}_{i,j+1/2}$ and $\mathbf{W}_{i,j+1/2}$ are obtained from $\mathcal{G}^+_{i,j+1/2}$ and $\mathcal{G}^-_{i,j+1/2}$ as

$$\mathbf{U}_{i,j+1/2} = \frac{1}{2B_{i,j+1/2}}\left(\mathcal{G}^+_{i,j+1/2} + \mathcal{G}^-_{i,j+1/2}\right), \qquad \mathbf{W}_{i,j+1/2} = \frac{1}{2}\left(\mathcal{G}^+_{i,j+1/2} + \mathcal{G}^-_{i,j+1/2}\right). \quad (34)$$

Note that the above local auxiliary variables, introduced to approximate the derivatives of the solution, are superficial and can be easily removed for linear problems. Clearly, the accuracy of the relaxation method will depend on the choice of the characteristic speeds $A_{i+1/2,j}$ and $B_{i,j+1/2}$ in (33) and (34), respectively.

ACKNOWLEDGEMENTS

Partial financial support from the the German Research Foundation (DFG) Grant DFG Schwerpunktprogramm 1253 and HE5386/6-1, /7-1, /8-1 and DAAD support with the PPP program is gratefully acknowledged. M. Seaïd is deeply grateful to the RWTH university at Aachen for their hospitality during a research visit there.

REFERENCES

1. Ambroso, A., Chalons, C., Coquel, F. Godlewski, G., Raviart, P.-A. and Seguin, N. *Relaxation methods and coupling procedures*, Internat. J. Numer. Methods Fluids, Vol. 56 (2008), pp. 1123-1129.
2. D.S. Balsara and C.W. Shu. Monotonicity Preserving Weighted Essentially Non-Oscillatory Schemes with Increasingly High Order of Accuracy. *J. Comp. Phys.*, 160:405–452, 2000.
3. M. Banda and M. Seaïd. Higher-Order Relaxation Schemes for Hyperbolic Systems of Conservation Laws. *J. Numer. Math.*, 13:171–196, 2005.
4. M.K. Banda and M. Herty and A. Klar, *Coupling conditions for gas networks governed by the isothermal Euler equations.*, NHM, 1(2006), pp. 295-314.
5. M.K. Banda and M. Herty and A. Klar, *Gas Flow in Pipeline Networks.*, NHM, 1(2006), pp. 41-56.
6. G. Bastin, B. Haut, J.-M. Coron and B. D'Andréa-Novel, *Lyapunov stability analysis of networks of scalar conservation laws*, Netw. Heterog. Media, **2** (2007) 751–759 (electronic).
7. R. M. Colombo and M. Garavello, *On the p-system at a junction*, Contemporary Mathematics, (2006).
8. R. M. Colombo and M. Garavello, *A well–posed Riemann problem for the p-system at a junction*, NHM, 1 (2006), pp. 495–511.

9. R. M. Colombo, M. Herty and V. Sachers, *On* 2×2 *conservation laws at a junction*, SIAM J. Math. Anal., Vol. 40 (2008), pp. 605–622
10. R. M. Colombo, G. Guerra, M. Herty and V. Sachers, *Modeling and Optimal Control of Networks of Pipes and Canals*, SIAM J. Control and Optimization, to appear (2009)
11. J. M. Coron, *Control and Nonlinearity*, Mathematical Surveys and Monographs, Vol. 136, AMS, Providence (2007).
12. J. M. Coron, B. d'Andréa-Novel, G. Bastin, *A strict Lyapunov functionfor boundary control of Hyperbolic systems of conservation laws*, IEEE Transactions on Automatic Control, Vol. 52(1), (2007)
13. J. M. Coron, G. Bastin, B. d'Andréa-Novel, *Dissipative boundary conditions for one dimensional nonlinear hyperbolic systems*, SIAM J. Control and Optimization, Vol. 47, (2008), pp. 1460–1498
14. M. Gugat, *Nodal control of networked hyperbolic systems*, AMO Advanced Modeling and Optimization, Vol. 7 (2005), pp. 1- 23
15. M. Gugat and G. Leugering, *Global boundary controllability of the de St. Venant equations between steady states*, Annales de l'Institut Henri Poincaré, Nonlinear Analysis, Vol. 20 (2003), pp. 1–11.
16. J. de Halleux, C. Prieur, J. M. Coron, B. d'Andréa-Novel, G. Bastin, *Boundary feedback control in networks of open channels*, Automatica, Vol. 39(8), (2003), pp. 1365–1376.
17. V. Dos Santos, G. Bastin, J.-M. Coron and B. d'Andréa Novel, *Boundary control with integral action for hyperbolic systems of conservation laws: stability and experiments*, Automatica J. IFAC, **44** (2008) 1310–1318.
18. R. Dressler, *Mathematical solution to the problem of roll-waves in inclined open channels*, Communication in Pure and Applied Mathematics, **2** (1949) 149–194.
19. Gottlieb S, Shu C.W, Tadmor E. Strong Stability Preserving High Order Time Integration Methods. *SIAM Rev.* 2001; **43**:89–112.
20. M. Herty and M. Seaid, *Simulation of transient gas flow at pipe-to-pipe intersections*, International Journal for Numerical Methods in Fluids, Vol. 56 (2008), pp. 485-506
21. M. Herty, A. Singh and M. Seaid, *A domain decomposition method for conservation laws with discontinuous flux function*, Appl. Numer. Math., Vol. 57 (2007), pp. 361–373
22. G.S. Jiang and C.W. Shu. Efficient Implementation of Weighted ENO Schemes. *J. Comp. Phys.*, 126:202–212, 1996.
23. S. Jin and Z. Xin. The Relaxation Schemes for Systems of Conservation Laws in Arbitrary Space Dimensions. *Comm. Pure Appl. Math.*, 48:235–276, 1995.
24. G. Leugering and E. J. P. G. Schmidt, *On the modeling and stabilization of flows in networks of open canals*, SIAM J. Control Opt., Vol. 41(1), (2002), pp 164–180.
25. T.–T. Li, *Exact controllability for quasilinear hyperbolic systems and its application to unsteady flows in a network of open canals*, Mathematical Methods in the Applied Sciences, Vol. 27 (2004), pp. 1089–1114.
26. T.–T. Li, *Exact boundary controllability of unsteady flows in a network of open canals*, Math. Nachr. 278 (2005), pp. 310-329.
27. R. LeVeque, *Finite Volume Methods for Hyperbolic Problems*, Cambridge University Press, New York, 2002
28. M. Seaïd and A. Klar. Asymptotic-Preserving Schemes for Unsteady Flow Simulations. *Computers & Fluids.*, 35:872–878, 2006.
29. M. Seaïd. High-Resolution Relaxation Scheme for the Two-Dimensional Riemann Problems in Gas Dynamics. *Numer. Methods for Partial Differential Equations.*, 22:397–413, 2006.
30. M. Seaïd. Non-oscillatory Relaxation Methods for the Shallow Water Equations in One and Two Space Dimensions. *Int. J. Num. Meth. Fluids*, 46:457–484, 2004.
31. C.W. Shu. Total-variation-diminishing time discretization. *SIAM. J. Sci. Stat. Comp.*, 9:1073–1084, 1988.
32. Osiadacz A.J. *Simulation and analysis of gas networks.* Gulf Publishing Company: Houston, 1989.